

AMERICAN
SCIENTIFIC
PUBLISHERS

Copyright © 2014 American Scientific Publishers

All rights reserved

Printed in the United States of America

Synthesis and Characterization of Ultra-Fine Colloidal Silica Nanoparticles

Mohd Qasim¹, J. Ananthaiah², S. Dhara², P. Paik¹, and D. Das^{1,*}¹*School of Engineering Sciences and Technology, University of Hyderabad, Hyderabad 500046, India*²*School of Physics, University of Hyderabad, Hyderabad 500046, India*

A facile synthesis of colloidal silica nanoparticles of various sizes, employing the hydrolysis and condensation of tetraethyl orthosilicate (TEOS) in absence of any surfactant, is reported. The surfactant-free colloids of SiO₂ nanoparticles with diameter ~5–6 nm are stable upto 50 days after synthesis. The effects of different reaction parameters (e.g., concentration of TEOS, water, alcohol and ammonia) on particle sizes have been investigated. Particle sizes have been found to increase with increasing TEOS and ammonia concentration but decrease with increasing water concentration. Obtained products have been characterized through XRD, UV-Vis spectrophotometry, FTIR, HRTEM and FE-SEM. The colloidal stability has been characterized by zeta potential and rheological measurements.

Keywords: Colloidal Silica, Rheology, Optical Properties, Silica Nanoparticles.

Delivered by Publishing Technology to: unknown
IP: 117.215.217.75 On: Fri, 17 Oct 2014 05:08:56
Copyright: American Scientific Publishers

1. INTRODUCTION

The colloidal silica nanoparticle is a stable dispersion of solid SiO₂ nanoparticles in liquid media. Monodisperse SiO₂ nanoparticles are one of the most attractive materials in colloidal science because of their unique properties, such as surface structure and functionality (–OH), optical properties, biocompatibility etc.¹ Surface functionalized SiO₂ finds application in electronics, sensors, catalysis, polishing, paints, fillers and pigments.^{2–5} Because of the biocompatible nature and ease of surface modification, amorphous SiO₂ nanoparticles are a potential tool in medical biotechnology and used in several applications including target drug and gene delivery,^{6–8} molecular bioimaging, labeling of bio-marker of infected cancer and tumor cells etc.^{7,8} However, SiO₂ nanoparticles play different roles in different applications and their response strongly depend on the size and distribution, shape and surface properties.²

Among various methods reported for SiO₂ nanoparticles preparation Stober's process is known to produce monodisperse particles.^{5,9} Stober process involves hydrolysis and condensation of alkoxide of Si in aqueous alcohol solution, where liquid ammonia is used as a morphological catalyst. The size of SiO₂ nanoparticles strongly depends on the reaction parameters such as, solvent,

catalyst, temperature, reaction time etc.¹⁰ SiO₂ nanoparticles of size less than 5 nm to several micrometers can be synthesized by microemulsion method,¹¹ organometallic sphere endotemplate method,¹² surfactant template method etc. These techniques can yield smaller size particles with narrow size distribution compared to those obtained from Stober process, but large amount of surfactant and co-stabilizers are used in these processes.¹³ Therefore, the particles require thorough purification before being employed for any specific application. Removing surfactant micelles from SiO₂ network structure is not an easy task since it can entrap the micelles due to the electrostatic interactions. Surfactant free SiO₂ nanoparticles, therefore, have a great promise in biological applications. Stober process generally produces larger size silica particles (0.05 to 2 μm).⁹ A number of research groups modified Stober process to achieve silica nanoparticles of size <10 nm,^{14–21} but to the best of our knowledge none of them have succeeded to achieve surfactant/metal ions free colloidal SiO₂ of size below 10 nm. Here, in this work, an effort has been made to synthesize colloidal SiO₂ nanoparticles of different sizes (5 to 30 nm) without the use of any surfactant or related compounds. The colloidal SiO₂ nanoparticles have been prepared only by varying the concentration of TEOS, H₂O, NH₃ using sonochemical synthesis followed by the Stober process. In the modified process very less TEOS has been

*Author to whom correspondence should be addressed.

used for all sets of experiments and has been added drop wise after diluting with absolute ethanol. Liquid ammonia has also been added drop wise in two steps to avoid sudden increase in particles size in all the experiments. To the best of our knowledge the present work is the first report on the synthesis of SiO_2 of particles sizes $\sim 5\text{--}6$ nm in absence of any surfactant. The stability of the SiO_2 colloids has been studied using zeta potential (ζ) and rheological property measurements. The changes in viscosity have been studied as a function of shear rate and temperatures. The rheological behavior of all the colloidal silica nanoparticles has been explained in terms of their morphology, zeta potential and compositions and has been reported in the articles.

2. EXPERIMENTAL DETAILS

2.1. Materials

Tetraethyl orthosilicate (TEOS, 99.99%, Sigma Aldrich), ammonia (25%, Qualigens), and ethanol (99.9%, Hangzhou) were used in these experiments without any purification. Deionized water was used in all experiments.

2.2. Synthesis of Colloidal Silica Nanoparticles Under Different Conditions

The experiments were performed using the precursor concentrations mentioned in Table I. All concentrations were calculated based on the final concentration in the reaction mixture. First, solution containing appropriate quantities of absolute ethanol, ammonia and deionized water was sonicated in a 50 Hz TRANS-O-SONIC sonicator for 10 minutes in 100 ml closed mouth beaker to ensure no evaporation of the solvent and complete mixing. Appropriate amount of TEOS in absolute ethanol was added to the above solution drop wise (0.03 ml/min) and after sonicating for 100 minutes again ammonia was added drop wise (0.05 ml/min) to promote the condensation reaction. Continuous sonication for about 70 minutes led to the formation of white turbid suspension of silica nanoparticles. Photograph of the as prepared colloidal silica nanoparticles after eight weeks of synthesis have been shown in Figure 1. Powder of silica nanoparticles were obtained by evaporating the solvent initially at 50°C for 2 hours and then at 150°C for 2 hours in hot air oven. The conversion of the reactants into silica nanoparticles has been estimated using the following formula,

Table I. Concentrations of the precursors used in different experiments.

Name of sample	Solvent	TEOS (M)	H ₂ O (M)	NH ₃ (M)
S1	Ethanol	0.044	5.55	0.441
S2	Ethanol	0.134	5.55	0.441
S3	Ethanol	0.268	5.55	0.441
S4	Ethanol	0.134	2.77	0.441
S5	Ethanol	0.134	8.33	0.441
S6	Ethanol	0.044	5.55	0.147
S7	Ethanol	0.044	5.55	0.735
S8	Isopropanol	0.044	5.55	0.735



Figure 1. Photograph of colloidal SiO_2 nanoparticles after eight week of synthesis. All the samples are found to be stable with time.

Yield (%)

$$= \text{Observed weight (g)} \times 100 / \text{Theoretical weight (g)}$$

where the theoretical weight of the sample was calculated based on 100% conversion of TEOS into SiO_2 .¹⁰ The yield (%) for each experiment is found to be $\sim 95\%$.

2.3. Characterization Techniques

Particle sizes, shape and morphology were measured using Transmission electron microscopy (FEI Tecnai T20G2 S TWIN TEM) and field emission scanning electron microscopy (Carl Zeiss Ultra 55 FESEM). A drop of dilute and well sonicated colloidal silica solution was placed on a carbon coated copper grid, the solvent was evaporated and the grid was examined by TEM. For the FESEM, a drop of sample was placed on carbon tape pasted on holder, solvent was evaporated and the particles were coated with ~ 10 Å thin gold layers before examining in FESEM. The particle size was estimated using analysis image processing software. The compositional analysis of the sample was carried out by a Horiba Energy Dispersive X-ray Micro-analyzer attached to a Hitachi S-3400N SEM. Crystal structure of the samples was analyzed by SAED pattern obtained from TEM and from XRD data. The as-prepared and calcined silica particles were analyzed by a Bruker D8 Advance X-ray Diffractometer with $\theta\text{--}2\theta$ geometry, using $\text{Cu K}\alpha$ radiation, in the 2θ range $5\text{--}50^\circ$. The optical absorption behavior was analyzed using a UV-Vis spectrophotometer (Perkin Elmer Lambda 35). Fourier transformed infrared (FT-IR) analysis was conducted on pellet made by mixing 1 mg of SiO_2 in 100 mg KBr using Perkin-Elmer 2000 FT-IR spectrometer. The Zeta potential and particle sizes of colloidal silica were measured by Zetasizer Ver. 6.20 (Malvern Serial Number: MAL1048519). Dynamic viscosity was measured using a standard rheometer (Anton Paar MCR 501) with controlled shear rate (CSR). The measuring system was a coaxial cylinder (CC-27). The temperature of the system was controlled using a Peltier device with an accuracy of $\pm 0.1^\circ\text{C}$.

3. RESULTS AND DISCUSSION

The effects of TEOS, H₂O and NH₃ with concentrations on particle sizes and shape have been studied. The concentrations of reactants and their effects on particle sizes are shown in Tables I and II respectively. It was observed from TEM (Fig. 2) and FESEM (Fig. 3) that the particle sizes of silica nanoparticles obtained from all the experiments to be very small. The largest particle size observed in this investigation is 31 ± 1.37 nm for as prepared sample S8. Particle size of 5.4 ± 0.61 nm is obtained for sample S6. About 2–3 micrographs of each sample were considered to obtain the mean particle sizes and ~ 150 particles were measured for each sample. To the best of our knowledge this synthesis procedure with optimized condition (sample S6) is the easiest way to produce ultrafine sized, highly pure and stable colloidal silica nanoparticles, without the use of any surfactant, template based technique, and metal salt catalyst, which cause contamination to the particles. Ultrafine silica nanoparticles are very prone to agglomeration mainly due to the hydrogen bonding present between the surface –OH groups and minimize the high surface energy. TEM and FESEM analysis of the 50 days aged colloidal silica show the same mean sizes of the particles as those of the freshly prepared samples.

3.1. Solid State Crystal Structure

The solid state phase structure of all the SiO₂ samples was checked by XRD with a CuK α radiation (CuK α = 1.540598 Å) at room temperature. Figure 4(a) shows the X-ray diffraction pattern of as prepared S1, S2, S3, S5, and S8 samples. XRD results show that all the SiO₂ samples are amorphous in nature as expected and reported by others.²² The broad diffraction peak at $2\theta = 23^\circ$ and absence of any diffraction peak from impurities confirmed the formation of pure amorphous silica nanoparticles. Same has also been confirmed from the SAED patterns (inset of TEM, Fig. 2).

The effect of calcination temperatures on the phase structure has also been studied. The XRD patterns of the representative sample S8, calcined at different temperatures varying from 150 °C to 1200 °C, are shown in Figure 4(b). All samples have been calcined for

2 1/2 hours. XRD pattern shows that silica nanoparticles are amorphous upto the calcination temperature of 900 °C. It is also found that with increasing calcination temperature the XRD peak intensity increases implying crystallization in silica phase. It is evident from the diffraction pattern that at 1000 °C amorphous silica transformed into crystalline (Cristobalite) silica.²³ The diffraction spectra of the samples calcined at 1100 and 1200 °C are almost similar in nature. The observed diffraction peaks at $2\theta = 21.88^\circ$ [101], 28.48° [111], 31.39° [102], and 36.193° [200] correlates well with the cristobalite tetragonal phase (Ref. JCPDF card number 89-3434). The crystallization temperature of amorphous silica reported else where is 1300 °C.²⁴ But, in this investigation the crystallization temperature is observed at around 1000 °C. The different synthesis route or different experimental conditions used in this study could lead to such difference in crystallization temperature. The crystallite size of all samples, calcinated at different temperatures, has been estimated from the XRD peak broadening using Scherrer's formula $d = 0.9\lambda/\beta \cos \theta$, where d is the crystallite size, λ is the wavelength of X-ray radiation (CuK α), θ is the Bragg angle and β is the full width at half maximum (FWHM) of the most intense diffraction peak.²⁵ The crystallinity and crystallite size increases with increase in calcination temperatures. Around 80% increase in crystallite size is observed in increasing the calcination temperature from 1000 °C to 1100°C (16.3 nm at 1000 °C to 29.2 nm at 1100 °C). Further increase in calcination temperature caused less effect on crystallite size. The crystallite size of the sample calcined at 1200 °C is ~ 31.1 nm.

3.2. FTIR Analysis

To confirm the chemical structure related to the functional groups and purity of the prepared samples FT-IR analysis was performed. The FTIR spectra of silica nanoparticles (S8) is shown in Figure 5. The intense and broad band appearing at ~ 1079 – 1167 cm⁻¹ is assigned to the asymmetric stretching vibrations of Si—O—Si bond.⁷ The absorption band at ~ 1079 cm⁻¹ is arising from asymmetric vibration of Si—O bond. The bands at ~ 960 cm⁻¹ and ~ 801 cm⁻¹ can be assigned to the asymmetric vibration of

Table II. Physical properties of colloidal silica nanoparticles, S1–S8.

Sample name	Mean particle size (nm)		Mean particle size (nm) by		Zeta potential (mV)	pH	Observed SiO ₂ concentration (mg/ml)	Theoretical SiO ₂ conc. (mg/ml)	Yield (%)
	by TEM	SD (nm)	FESEM	SD (nm)					
S1	9.4	0.65	11.3	2.25	-20.1	9.45	2.57	2.7	95.1
S2	12.9	0.78	13.7	1.42	-21.9	9.54	7.4	8.1	91.5
S3	12.2	0.84	12.9	1.77	-21.7	9.48	15.0	16.1	93.1
S4	14.9	0.91	15	1.41	-32.4	9.54	7.5	8.1	92.8
S5	10.2	0.80	10.2	1.22	-25.4	9.89	7.2	8.1	89.1
S6	5.4	0.61	6	1.25	-36.9	9.96	2.5	2.7	92.5
S7	20.9	2.41	26.4	1.92	-32.7	10.23	2.6	2.7	96.3
S8	31	1.37	37.5	7.00	-30.9	10.21	2.47	2.7	91.4

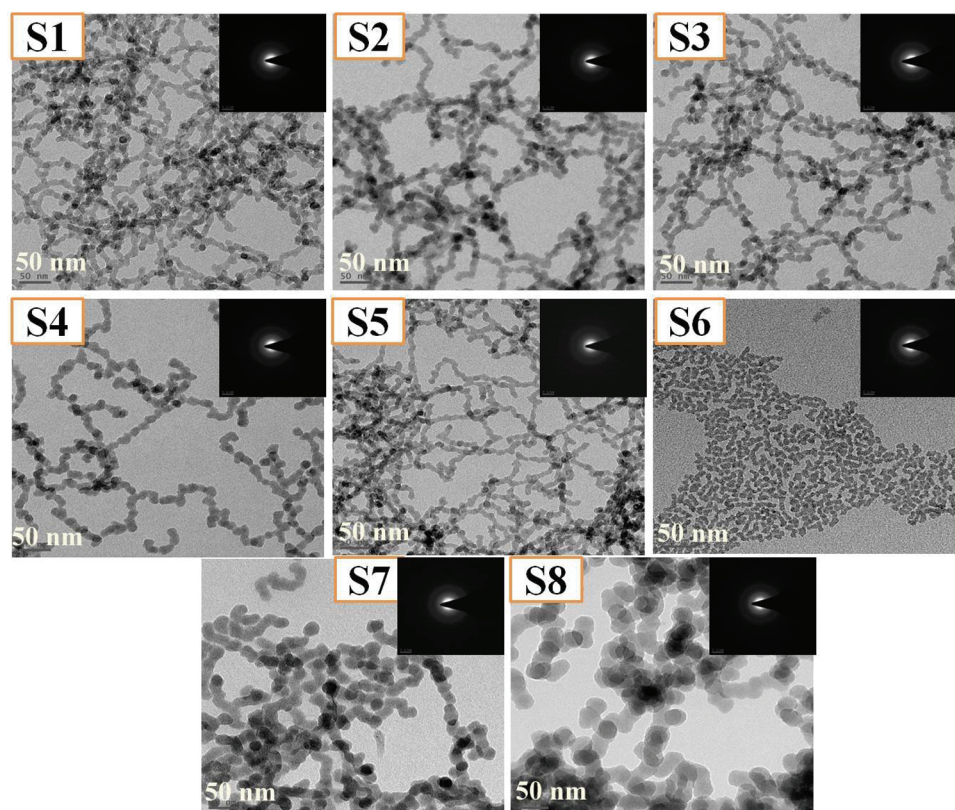


Figure 2. TEM images and SAED pattern (inset) of all (S1–S8) SiO₂ nanoparticles. The scale bar is 50 nm.

Si—OH bond,¹⁸ and symmetric vibration of Si—O bond respectively. The band at $\sim 468\text{ cm}^{-1}$ corresponds to the bending mode of Si—O—Si bond. An intense characteristic absorption band around $3300\text{--}3500\text{ cm}^{-1}$ arises due to the O—H stretching vibration mode of Si(OSi)_n(OH)_{4-n} ($n = 2\text{--}4$) linkage of the solid state network structure of silica or due to the unbounded absorbed water.^{26–28} The band at $\sim 1631\text{ cm}^{-1}$ is due to scissor bending vibration of molecular water.²⁹

3.3. Effect of TEOS Concentration on the Size of Particles

The effect of TEOS concentration on the size of SiO₂ nanoparticles is controversial in some literature it is found that there is no significant effect of TEOS concentration on particle sizes⁹ but, Bogush et al. and a group of researchers^{3,4,10,15} reported that increasing particles sizes with increasing TEOS concentration. Helden et al.³⁰ however reported that high TEOS concentration can decrease the particle sizes also. In the present study, increased size of the silica nanoparticles was observed with increasing TEOS concentration (0.044–0.268 M), with 5.55 M water, and 0.441 M ammonia concentration (samples: S1, S2, S3). Being the source of monomer, concentration of TEOS will determine the concentration of the nuclei/primary particles present in the system.⁴ Hence, the increase in particle size is attributed to the increase in

concentration of primary particles at the induction period, i.e., [primary particles] \propto [TEOS]. Induction period is the time period when generation of nuclei takes place from the supersaturated solution and induces formation of primary particles. Therefore, TEOS concentration determines the concentration of primary particles, but at the same time the concentration of these primary particles determines the subsequent growth of these particles. TEOS was diluted with ethanol and was added to the reaction system drop wise very slowly in order to promote the formation of smaller particles. Figure 6 shows the effects of TEOS concentration on size of silica nanoparticles. The particle size increases with increasing TEOS concentration up to 0.134 M and after that it does not change much. The particle size is seen to vary from 9.4 ± 0.6 to 12.9 ± 0.7 nm, measured by TEM, and 11.3 ± 2.2 to 13.7 ± 1.4 nm, measured by FESEM. Both the TEM and FESEM analysis show that the particles are almost monodispersed. The particles sizes for all the samples are mentioned in Table II.

3.4. Effect of Water Concentration on Size of Particles

In the present study, decrease in size of the silica nanoparticles was observed with increasing water concentration in the range 2.77–8.33 M, with 0.441 M ammonia, and 0.134 M TEOS concentration (sample S4, S2, S5).

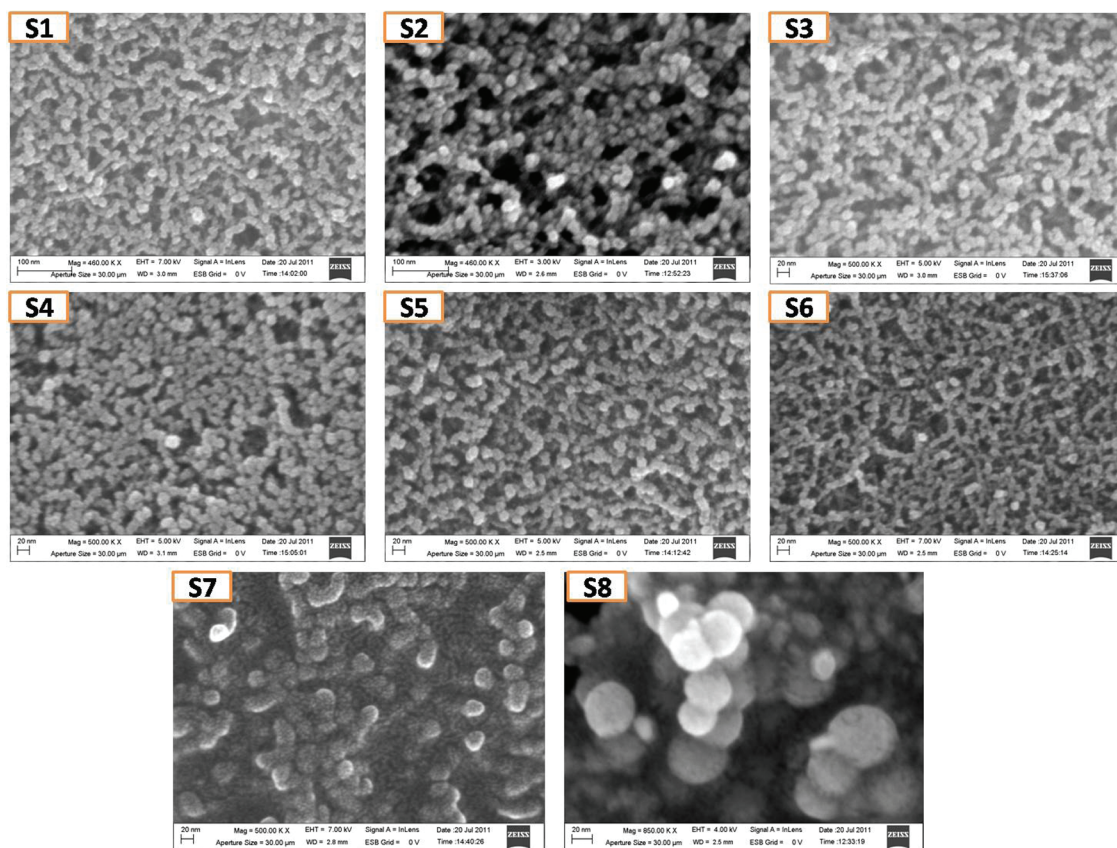


Figure 3. FESEM images of SiO₂ nanoparticles (S1–S8).
 Delivered by Publishing Technology to: unknown
 217.75 On: Fri, 17 Oct 2014 05:08:56
 Copyright: American Scientific Publishers

The obtained result is in good agreement with the results reported by Rahman et al.⁴ Figure 6 illustrates the trend in particle sizes with increasing water concentrations. It is observed that as the R value (water/TEOS ratio) increases the particles size also decreases. The R values for samples S4, S2 and S5 are 20.67, 41.41 and 62.16, respectively. Generally, water promotes hydrolysis and condensation reaction resulting in increase in particle sizes. At higher H₂O concentration the oligomers in reaction solution get diluted, resulting in the formation of smaller particles. In the present investigation, the decrease in size of the silica nanoparticles with increasing water concentration may be associated with the dilution of silicate concentration which slows down the hydrolysis and condensation reaction, resulting in restricted particle growth. Matsoukas and Gulari³¹ have also reported that the increase in water concentration yields smaller particles. The estimated particle size is seen to vary from 14.9 ± 0.9 – 10.2 ± 0.8 nm. The particle size data obtained from TEM (Fig. 2) correlates well with those obtained from FESEM (Fig. 3). Although the average particle size is seen to decrease with increasing water concentration and their tendency to form a chain like structure (by joining many single particles) increases with increasing water concentration.

3.5. Effect of Ammonia Concentration on the Size of Particles

Normally acid catalyzed hydrolysis is a very slow process compared to the basic one and hence base catalyzed process is preferable to synthesize ultra-fine monodispersed SiO₂ nanoparticles. In this work NH₃ is used as a catalyst for hydrolysis and condensation of TEOS in ethanol. It is worth mentioning that the higher NH₃ and water content in the reaction mixture increase the rate of hydrolysis.⁷ It has been found in earlier work that slow drop wise addition of NH₃ for a longer period controls the growth and limits the size of particles, whereas faster rate of addition reverse the effect and produce bigger size particles.⁹ On addition of NH₃ the pH of the solution increases and leads to the formation of large number of SiO₂ nuclei, which subsequently grow into silica particles. From Figure 6, it is clearly observed that as the NH₃ is increased from 0.147 M to 5.55 M the particle size increased from 6 nm to ~26.4 nm in presence of 0.044 M TEOS and 5.55M H₂O in the fixed volume of EtOH. (Samples S6, S1, S7). The probable reason for this is that as the NH₃ increases the rate of hydrolysis of TEOS increases to form $[\text{Si}(\text{OC}_2\text{H}_5)_{4-x}(\text{OH})_x]$, which subsequently condenses to produce large number of oligomers leading to the formation of larger sized particles.^{2,4} At very low

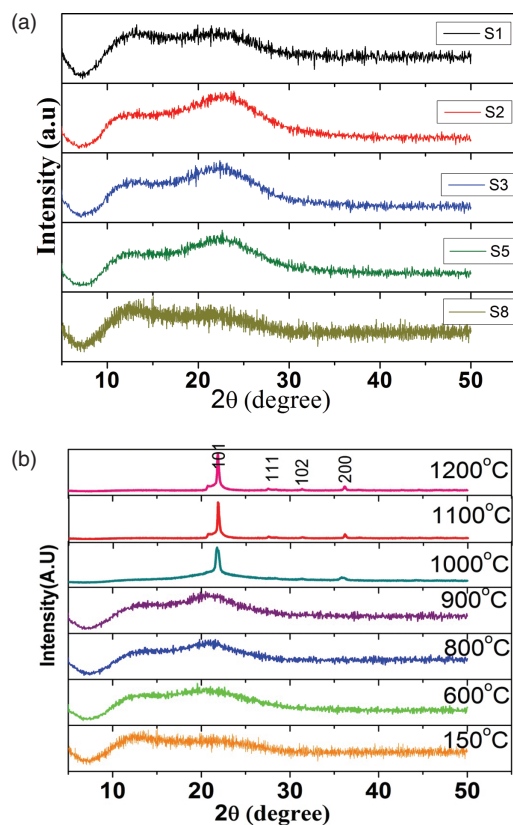


Figure 4. (a) X-ray diffraction patterns of as prepared S1, S2, S3, S5, and S8 SiO₂ nanoparticles; (b) XRD patterns of SiO₂ nanoparticles (S8) calcined at different temperatures.

NH₃ concentration ultrafine silica nanoparticles of dimensions 5–6 nm are obtained. This finding will help other researchers to prepare ultra fine silica nanoparticles without using any surfactant.

3.6. Effect of Other Alcohols on the Size of Particles

To observe the effect of solvent on the particle sizes, two different types of alcohols, such as ethanol (sample S7), and isopropanol (sample S8), were chosen keeping all the other experimental conditions constant (see Table I).

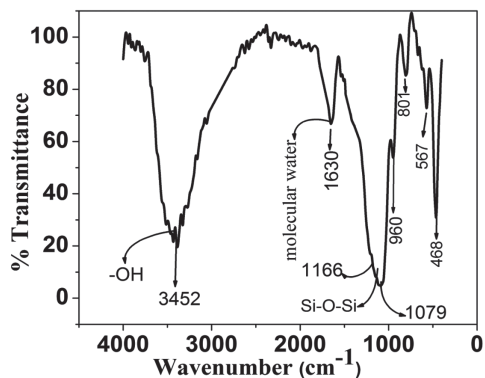


Figure 5. FT-IR spectra of as prepared SiO₂ nanoparticles (S8).

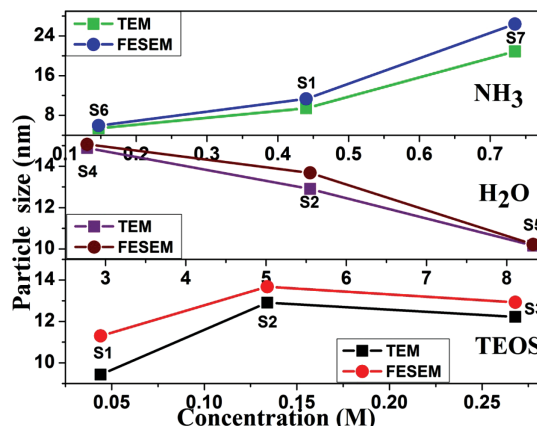


Figure 6. Effect of precursors (TEOS, H₂O and NH₃) concentration on size of SiO₂ nanoparticles. The filled squares represent estimated size from TEM data and filled circles that from FESEM data.

From TEM analysis it is observed that the size of SiO₂ particles increases from 21 nm, obtained in EtOH, to 31 nm obtained in isopropanol. Similar results have also been reported by Wang et al.³ where it was observed that as the chain length of the alkyl group increases the dielectric constant of the solvent decreases, which led to the increase in particle sizes. It is worth mentioning that the dielectric constants of ethanol and isopropanol are ~24.3 and 19.9, respectively. The dominance of van der Waals attractive forces or static repulsive forces between the nuclei or primary particles depends on the dielectric constant of the solvent. In a solvent with low dielectric constant the attractive force between the nuclei dominates over the static repulsive forces and hence promotes the reaction kinetics with subsequent particle growth.^{3,19}

3.7. Zeta Potential

Zeta potential measurement was carried out to check the stability of colloidal silica nanoparticles and is seen to vary from -20.1 to -36.9 mV depending of the particle size and morphology and is mentioned in Table II.

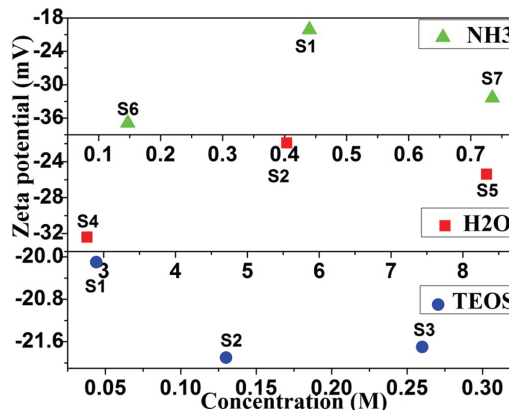


Figure 7. Variation of zeta potential of all colloidal SiO₂ with reactant concentrations (TEOS, H₂O and NH₃) for colloidal SiO₂ nanoparticles.

The zeta potential values of the samples suggest that SiO_2 nanoparticles are moderately stable in suspension. Samples S1, S2, S3, and S5 have lower zeta potentials than samples S4, S6, S7, and S8. It is observed (in Tables I and II) that a changes in particles sizes (9–12 nm) and zeta potentials (Fig. 7) are weakly dependent on changes in TEOS concentration. Change in water concentration from 2.77 M (S4) to 5.55 M (S2) changes the zeta potential value from -32.4 to -21.9 mV. Further increase in water concentration does not affect the zeta potential of colloidal SiO_2 (S5). With increasing ammonia concentration, zeta potential decreases at beginning (-36.9 mV for S6 to -20.1 mV for S1) followed by a rapid increase to -32.7 mV for S7 with further increase in the ammonia concentration. NH_4OH produces hydroxyl ions, which get adhered to the silica particle surfaces and helps in stabilizing the colloids by static repulsion force against van der Waals forces of attraction. However, the change in zeta potential depends on the particle sizes and the surface charge density, which is strongly associated with the pH of the solution.

3.8. Rheological Measurements

Dynamic viscosity of the colloidal silica was measured using a standard rheometer (Anton Paar MCR 501) with controlled shear stress (CSS). The measuring system was

a coaxial cylinder (CC-27). The temperature of the system was controlled using a Peltier device with an accuracy of ± 0.1 °C. In Figure 8(a) the variation of dynamic viscosity is shown as a function of shear rate. In the low shear rate range (< 200 s^{-1}) the dynamic viscosity varies from 1.4 to 2 mPa s depending on the sample and does not change with shear rate. Thus, in the low shear rate range all the samples show behavior of a typical Newtonian fluid. It is observed that S5 and S3 exhibit larger viscosity than other samples. This is because of higher concentration of silica (S3) and water (S5) in these samples as both lead to extensive networking or formation of chain like structure as discussed later. It was observed that the samples S4, S2, and S5, because of their increasing water contents, show increasing trend in viscosity. Sample S5 shows larger viscosity than S4 and S2. It was confirmed by TEM that as the amount of water content increases the particles tend to form longer chain or networks by joining with each other. This is due to increasing tendency of hydrogen bonding between particles and formation of chain like structure that gives rise to larger viscosity. Sample S1, S6, and S7 show almost similar viscosity because they have same amount of water and silica content.

In the high shear rate range i.e., beyond 200 s^{-1} , the viscosity abruptly changes slope and increases with the increasing shear rate showing shear thickening behavior. Similar type of shear thickening behavior is reported on colloidal dispersion of silica nanoparticles.^{32,33} It was suggested that in polar liquid silica nanoparticles could interact via hydrogen bonding and hence they have strong tendency to form microstructures. In the present samples the solvent contains ethanol and water and both of them are polar liquids. Hence there is a strong tendency to form nanostructures or nanoclusters due to hydrogen bonding as discussed earlier. In the low shear rate range the equilibrium nanostructure remains undisturbed and the samples behave as a stable non-flocculated sol with constant viscosity. As the shear rate is increased the short-range hydrodynamic lubrication forces can bring the nanoclusters closer and facilitate the microstructure formation and hence can form a gel like structure. This can lead to higher rates of energy dissipation and abrupt increase in the dynamic viscosity. Further investigation is needed to shed more light on the shear thickening behavior of the samples. Since the viscosity of colloids strongly depends on temperature, temperature dependence of viscosity has been measured for two samples, namely S1 and S4 and a typical variation is shown in Figure 8(b). The viscosity decreases for both the sample rapidly with the increasing temperature and shows an Arrhenius type of behavior i.e., $\eta = \eta_0 \exp [E/RT]$ where E is the activation energy and η_0 is the pre-exponential factor. The logarithm of the viscosity with inverse of the temperature for the two samples is shown in Figure 8(b) (inset). The activation energies for the two samples, S1 and S4 are 4031 and 3776 cal/mol

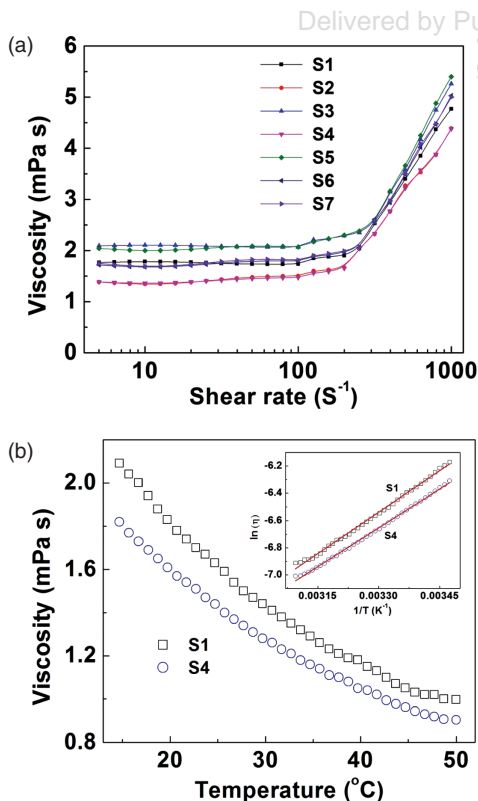


Figure 8. (a) Variation of shear viscosity of colloidal SiO_2 nanoparticles as function of shear rate at 27 °C. (b) Temperature variation of shear viscosity for two colloidal SiO_2 samples namely S1, S4 at shear rate 5 s^{-1} and inset shows the Arrhenius behavior of viscosity.

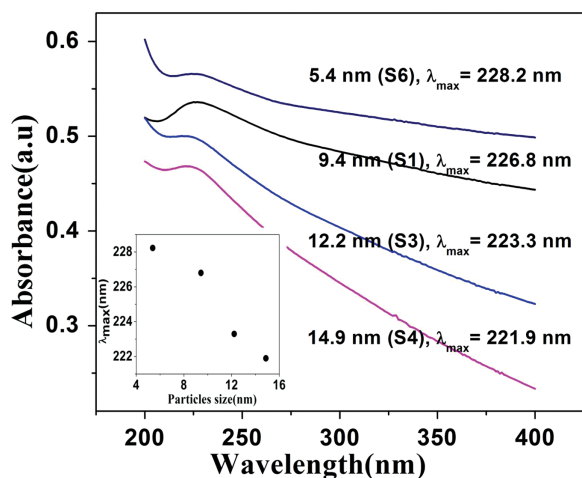


Figure 9. UV-vis absorption spectra of colloidal SiO₂ nanoparticles sample S1, S3, S4 and S6 and variation of λ_{\max} with particles size (inset).

respectively. These values are comparable to the activation energy reported in the binary mixture of pure water and ethanol with similar concentration.³⁴

3.9. UV-Vis Spectroscopy

In silica nanoparticles the optical phenomena is related to the presence of different defects due to incomplete formation of Si—O—Si tetrahedral network at the silica surface, such as oxygen and silicon vacancies.³⁵ To study the effect of particles size on electronic absorption behavior, UV-Vis spectra of powder samples S6 (5.4 nm), S1 (9.4 nm), S3 (12 nm), S4 (15 nm) have been taken after dispersing in water. UV-vis absorption spectra of different sizes of silica nanoparticles showed a single λ_{\max} at 221.9–228.3 nm (Fig. 9). This region corresponds to energy range 5.59–5.43 eV. The above absorption range may be attributed to the presence of surface paramagnetic E' centers, such as paramagnetic positively charged oxygen vacancies ($\equiv\text{Si}\cdot\text{Si}\equiv$), or neutral dangling Si bonds ($\equiv\text{Si}\cdot$).³⁶ A slight red shift was observed in λ_{\max} with decrease in size of the silica nanoparticles from 14.9 nm to 5.4 nm. The λ_{\max} is varying from 228.3 to 221 nm for increasing the particles size from 5.4 to 15 nm. The variation in λ_{\max} with increasing silica particles sizes is shown in the inset of Figure 9. A linear decrease in λ_{\max} is observed with increasing size of the silica nanoparticles. Rahman et al.³⁶ explained the decrease in λ_{\max} in terms of intra-particle stabilization of E' centers due to the presence of larger number of neighboring atoms and silanol groups per nm² of larger silica nanoparticles. The stability of E' centers is seen to increase linearly with increase in particle sizes. The partially negative charge oxygen atom of —OH could attract positively charged paramagnetic defects resulting in stabilization of the defects. After stabilization a higher energy is required for the excitation of electron from the E' centers. The observed results are consistent with that of Rahman et al.³⁶

4. CONCLUSIONS

Ultra-fine colloidal silica nanoparticles of different sizes and morphology have successfully been synthesized by a modified Stober process using a low frequency ultrasonic bath. Obtained sizes varied from 5–31 nm. Colloidal silica nanoparticles with such tight distribution in sizes, which conveniently fall into primary size range, have been prepared without the use of any surfactant or metal salt as catalyst. The effect of reactants concentration (TEOS, water, ammonia and alcohol) on particle sizes has been investigated. The particle sizes are seen to increase with increasing TEOS and ammonia concentration but decrease with increasing water concentration. Alcohol of larger molecular weight enhances the particle growth. The maximum in UV-Vis absorption spectra is seen to shift at higher wavelengths with decreasing size of the silica nanoparticles. At low shear rate ($<200\text{ s}^{-1}$), a typical Newtonian behavior is observed for all the colloidal silica nanoparticles, but at high shear rate ($>200\text{ s}^{-1}$), a shear thickening behavior is observed.

Acknowledgment: Mohd Qasim greatly acknowledges the financial support obtained from UGC in the form of MANF fellowship in carrying out this research work. The technical support received from the Centre of Excellence in Materials Science (Nanomaterials) Aligarh Muslim University, School of Engineering Sciences and technology (SEST), Centre for Nanotechnology and School of Physics at the University of Hyderabad is greatly appreciated.

References and Notes

1. R. K. Iller, *The Chemistry of Silica and Silicates*, Eng. Aspects Wiley, New York (1979), p. 132.
2. S. K. Park, K. D. Kim, and H. T. Kim, *Coll. Surf. A* 197, 7 (2002).
3. X. D. Wang, Z. X. Shen, T. Sang, X. B. Cheng, M. F. Li, L. Y. Chen, and Z. S. Wang, *J. Colloid Interface Sci.* 341, 23 (2010).
4. I. A. Rahman, P. Vejayakumar, C. S. Sipaut, J. Ismail, M. A. Bakar, R. Adnan, and C. K. Chee, *Colloids Surf., A: Physicochem. Eng. Aspects* 294, 102 (2007).
5. H. Lim, J. Lee, J. Jeong, S. Oh, and S. Lee, *Engineering* 2, 998 (2010).
6. F. Muhammad, M. Guo, W. Qi, F. Sun, A. Wang, Y. Guo, and G. Zhu, *J. Am. Chem. Soc.* 133, 8778 (2011).
7. S. Santra, P. Zhang, K. Wang, R. Taped, and W. Tan *Anal Chem.* 73, 4988 (2001).
8. S. Bonacchi, D. Genovese, R. Juris, M. Montalti, L. Prodi, E. Rampazzo, and N. Zaccheroni, *Angew Chem. Int. Ed.* 50, 4056 (2011).
9. W. Stöber, A. Fink, and E. Bohn, *J. Colloid Interface Sci.* 26, 62 (1968).
10. K. S. Rao, K. Hami, T. Kodaki, K. Matsushige, and K. Makino, *J. Colloid Interface Sci.* 289, 125 (2005).
11. T. Aubert, F. Grasset, S. Mornet, E. Duguet, O. Cador, S. Cordier, Y. Molard, V. Demange, M. Mortier, and H. Haneda, *J. Colloid Interface Sci.* 341, 201 (2010).
12. K. Suzuki, S. Sato, and M. Fujita, *Nature Chemistry* 2, 25 (2010).
13. K. S. Finnie, J. R. Bartlett, C. J. A. Barbe, and L. Kong, *Langmuir* 23, 3017 (2007).
14. G. H. Bogush, M. A. Tracy, and C. F. Zukoski IV, *J. Non-Cryst. Solids* 104, 95 (1988).

15. H. G. Bogush and C. F. Zukoski, *J. Coll. Interf. Sci.* 142, 19 (1991).
16. S. Roy, S. Bandyopadhyay, and D. Chakravorty *J. Mater. Sci. Lett.* 15, 1872 (1996).
17. S. L. Chen, *Colloids Surf. A* 142, 59 (1998).
18. N. Venkatathri, *Indian Journal of Chemistry* 46 A, 1955 (2007).
19. H. C. Wang, C. Y. Wu, C. C. Chung, M. H. Lai, and T. W. Chung, *Ind. Eng. Chem. Res.* 45, 8043 (2006).
20. M. Jafarzadeh, I. A. Rahman, and C. S. Sipaut, *Journal of Sol Gel Science and Technology* 50, 328 (2009).
21. E. Murray, P. Born, A. Weber, and T. Kraus, *Adv. Eng. Mater.* 12, 374 (2010).
22. K. Qi, X. Chen, Y. Liu, J. H. Xin, C. L. Makb, and W. A. Daouda, *J. Mater. Chem.* 17, 3504 (2007).
23. C. H. Kim and T. Oh, *Bull. Korean Chem. Soc.* 32, 3483 (2011).
24. O. Sneh and S. George, *J. Phys. Chem.* 99, 4639 (1995).
25. J. A. Khan, M. Qasim, B. R. Singh, S. Singh, M. Shoeb, W. Khan, D. Das, and A. H. Naqvi, *Spectrochim. Acta, Part A: Molecular and Biomolecular Spectroscopy* 109, 313 (2013).
26. P. Paik, A. Gedanken, and Y. Mastai, *ACS Appl. Mater. Interfaces* 8, 1834 (2009).
27. P. Paik, A. Gedanken, and Y. Mastai, *Microporous Mesoporous Mater.* 129, 82 (2010).
28. P. Paik, Y. Mastai, I. Kityk, P. Rakus, and A. Gedanken, *J. Solid State Chem.* 192, 127 (2012).
29. A. Beganskienė, V. Sirutkaitis, M. Kurtinaitienė, R. Juškėnas, and A. Kareiva, *Mater. Sci.* 10, 1320 (2004).
30. A. K. Van Helden, J. W. Jansen, and A. Vrij, *J. Colloid Interface Sci.* 81, 354 (1981).
31. T. Matsoukas and E. Gulari, *J. Colloid Interface Sci.* 124, 252 (1988).
32. S. R. Raghavan, H. J. Walls, and S. A. Khan, *Langmuir* 16, 7920 (2000).
33. B. J. Maranzano and N. J. Wagner, *J. Phys. Chem.* 117, 10291 (2002).
34. R. Belda, J. V. Herraiez, and O. Diez O, *Phys. Chem. Liq.: An International Journal* 42, 467 (2004).
35. I. A. Rahman and P. Vejayakumaran, *Journal of Nanomaterials* 2012, 15 (2012).
36. I. A. Rahman, P. Vejayakumaran, C. S. Sipaut, J. Ismail, and C. K. Chee, *Mater. Chem. Phys.* 114, 328 (2009).

Received: 26 March 2014. Accepted: 29 April 2014.

Delivered by Publishing Technology to: unknown
IP: 117.215.217.75 On: Fri, 17 Oct 2014 05:08:56
Copyright: American Scientific Publishers